Applied Catalysis B: Environmental 325 (2023) 122315

Contents lists available at ScienceDirect

Applied Catalysis B: Environmental

journal homepage: www.elsevier.com/locate/apcatb

Site-selective photocoupled electrocatalytic CO_2 reduction over efficient Al-oxo chain based-porphyrin framework

Keke Wang [a], Yang Liu [a], Jihu Kang [a], Yanfang Zhang [a], Qingmei Wang [a], Long Chen [a], Qiyou Wang [b], Bao Liu [b], Min Liu [b], Xiaoqing Qiu [a], Wenzhang Li [a,c,*], Jie Li [a,**]

[a] School of Chemistry and Chemical Engineering, Central South University, Changsha 410083 China
[b] Hunan Joint International Research Center for Carbon Dioxide Resource Utilization, School of Physics and Electronics, Central South University, Changsha 410083, China
[c] Hunan Provincial Key Laboratory of Efficient and Clean Utilization of Manganese Resources, Central South University, Changsha 410083, China

ARTICLE INFO

Keywords:
Al-oxo chain based-porphyrin framework
Atomic metal sites
Electronic structure
Photo-coupled electrocatalysis
CO_2 reduction

ABSTRACT

Photo-coupled electrocatalytic CO_2 reduction is an emerging method to promote energy efficiency of electrocatalytic CO_2 reduction. However, precisely designing a precatalysts with site-selectivity for efficient photo-coupled electrocatalytic CO_2 reduction is still a challenge. Here, a photo-coupled electrocatalyst bearing aluminum (Al)-oxo chain as metal node and transition metal sites as metal center, is dedicated to reducing CO_2 for the first time. A satisfactory CO_2-to-CO conversion is achieved for Al-PMOF(Co), showing a Faradaic efficiency as high as ~90% and a long-term stability over 35 h under visible light. The improved performance stem from Al-oxo chain imparting high stability, atomic Co site expediting charge transfer rate (K_{ct}) and visible light accelerating charge transfer across interface. Theoretical calculations and *in situ* reflection infrared spectroscopy show that the $3d_{z^2}$ orbital of atomic Co site exists a large resonance with the 2p orbital of *COOH intermediate, thus inducing CO_2 reduction though a favorable pathway.

1. Introduction

Electrochemical conversion CO_2 toward high-value chemicals is a promising technology to mitigate the excessive CO_2 emissions and store renewable electricity [1–3]. Despite many studies have committed to this field, some obstacles, such as the relatively low efficiency and selectivity, are still existed [4–6]. In order to decrease the side effect, external field is proposed to perfect the energy efficiency and intrinsic activity. As we all know, light irradiation possibly has an impact on electronic properties of some electrocatalysts, such as accelerating electron transfer and lowering the activation barriers between molecular catalysts and CO_2 binding [7–10]. All these factors can influence the catalytic pathways and activity. Therefore, electrocatalytic CO_2 reduction when coupled with photon energy (called photo-coupled electrocatalytic CO_2 reduction) is a promising way to further improve CO_2 reduction performance. However, photoelectrochemical (PEC) CO_2 reduction on traditional p-type semiconductors (such as metal oxide, metal chalcogenide) is challenging resulting from severe photocorrosion, leading to poor stability in aqueous solution. More seriously, the active site of semiconductors would be deactivated due to their instability in aqueous electrolyte, finally leading to a sharp decline in reduction efficiency [11–14]. Considering that, it is of supreme to seek new high-stability photo-coupled electrocatalyst with specific active site for efficient CO_2 conversion.

It is widely recognized that chlorophyll converts CO_2 into glucose through photosynthesis, continuously providing energy and resources for the entire ecosystem [15,16]. Porphyrins, as important part of chromophore of chlorophyll, is a photosensitive 18π aromatic macrocycle, thus chosen as light exciters in intrinsic structures. Moreover, porphyrins also possess predictable rigid structures and photochemical electron-transfer ability, making the electronic structure alter under light irradiation [17–19]. Thus, porphyrin will be a promising candidate for realizing photocoupled electrocatalytic CO_2 reduction reaction. Among numerous porphyrin structures, a aluminum (Al) mode-based porphyrin framework (Al-PMOF), characterized by the four carboxylate groups coordinated to eight Al mode [20,21], is a very appealing

* Corresponding author at: School of Chemistry and Chemical Engineering, Central South University, Changsha 410083 China.
** Corresponding author.
E-mail addresses: liwenzhang@csu.edu.cn (W. Li), lijieliu@csu.edu.cn (J. Li).

https://doi.org/10.1016/j.apcatb.2022.122315
Received 18 September 2022; Received in revised form 9 December 2022; Accepted 18 December 2022
Available online 20 December 2022

photoactive material due to its high thermal and chemical stabilities. The stability of framework depends on the inorganic brick and the strength of the inorganic brick and the linker [22]. The Al-based metal organic frameworks (MOFs) present more remarkable thermal and chemical stabilities than Cr-or Zr-based MOFs [23,24] due to the stronger strength of the Al-O bond (514 kJ/mol) compared with Cr-O bond (447 kJ/mol). Moreover, the thermal stability of Al-based MOF can venture far beyond other MOFs (350–400 °C) [25]. Besides, Al-PMOF possesses an ideal CO_2 adsorbaphore distance of 6.5–7.0 Å compared with other metals (such as Zn, Cu, Cr, Zr, Ni, Ba etc) [26], which can realize the carbon capture and storage. This function of Al-PMOF will be expected to finish the whole process of CO_2 conversion (from CO_2 capture, storage to forming hydrocarbon products). Thus, Al-PMOF will be a very potential material for entire CO_2 reduction. So far, the investigation on Al mode-based PMOF for CO_2 reduction remain scarce and highly desirable.

Apart from the above metal mode, active-site design is of utmost importance for CO_2 activation and the intermediates adsorption [27–29]. Of late years, a series of transition metal active sites (such as Fe, Co, Ni, Cu, etc.) have been introduced into porphyrin units for improving the activity and selectivity of electrocatalytic CO_2 reduction [30]. However, the site-selectivity in porphyrin framework is still controversial. For instance, Wang et al. found that among different transition metal sites, Co site anchored on Zr_6 clusters based porphyrin framework (PCN-222) presented the best selectivity for CO_2-to-CO conversion [31]. Guo et al. found that Fe site on an indium–porphyrin framework (In-PMOF) exhibited better performance of CO_2 reduction to CO [32]. More recently, it is found that Co site on MOF-525 composed of Zr_6-cluster-porphyrin framework exhibited ideal CO_2-to-CO conversion while Mn, Fe, Ni, and Cu sites dominated hydrogen evolution reaction (HER) over the CO_2 reduction reaction [33]. For Al-PMOF constituted by Al-oxo mode and tetra-carboxylated organic ligands, the site-selectivity is also unpredictable. Considering pristine Al-PMOF lacks of sufficient active sites for CO_2 reduction, the introduction of extra single metal active sites and studying the site-selective details on Al mode-based MOFs is of paramount necessity for realizing a high-efficiency and stable CO_2 reduction reaction.

Motivated by these findings, we targeted a high-efficiency and stable Al-based porphyrinic metal-organic framework (Al-PMOF) with different metal centers (Fe, Co, Cu) as CO_2 reduction photo-coupled electrocatalysts for the first time, to the best of our knowledge. The experimental results show that a satisfactory CO_2-to-CO conversion is achieved for Al-PMOF(Co), showing a Faradaic efficiency of CO as high as ~90% under visible light. Moreover, Al-PMOF(Co) exhibits long-term stability without performance decay over 35 h. Further, Al-PMOF(Co) exhibits a 2.7-fold higher photocurrent density (-4.3 mA/cm^2) at -0.8 V vs. RHE compared with Al-PMOF. Simultaneously, density functional theory (DFT) calculations demonstrated that Al-oxo chain based PMOF with tunable atomic metal site Co (Al-PMOF(Co)) can significantly lower the energy barrier of CO_2 and *COOH intermediate adsorption or activation. Furthermore, Al-oxo chain based PMOF with atomic Co site makes Co $3d_z^2$ orbital generate a stronger combination with *COOH, thus helping to the CO_2 activation and the following CO_2 reduction. Kinetic characterization of charge transfer and theoretical calculation indicates that the introduced visible light can accelerate the electron-flow, thus improving CO_2 reduction efficiency.

2. Experimental methods

2.1. Chemical and materials

The chemicals were purchased from the commercial suppliers and received without further purification. 4,4′,4‴-(porphine-5,10,15,20-tetrakis (98%+, Adamas). Aluminium chloride hexahydrate ($AlCl_3$•$6H_2O$), ferrous acetate tetrahydrate ($Fe(CH_3COO)_2$•$4H_2O$), copper acetate monohydrate ($Cu(CO_2CH_3)_2$•H_2O), cobalt acetate tetrahydrate ($Co(CH_3COO)_2$•$3H_2O$) were purchased by Sinopharm Chemical Reagent Co., Ltd. During the whole experiment, deionized water was provided as water. Carbon paper was utilized as all working electrodes. Then, the carbon papers were previously ultrasonically cleaned by acetone, ethanol for 15 min, respectively.

2.2. Synthesis of Al-PMOF

Al-PMOF was synthesized by adapting from the literature [26]. Typically, 100 mg (0.126 mmol) 4,4′,4‴-(porphine-5,10,15,20-tetrakis (benzoic acid) (H_2TCPP) were introduced into 10 mL of deionized water and stirred for 10 min. Then, a 10 mL aliquot of 0.025 M $AlCl_3$•$6H_2O$ solution was added into the above solution followed by 10 min stirring and 5 min sonication to make a homogeneous solution. Afterwards, the solution was transferred into a Teflon lined autoclave and heated at 180 °C for 24 h. Finally, the solution was allowed to cool with a cooling rate of 1 K min^{-1} to room temperature. The solid was recovered by filtration, washed 3 times with DMF, once with acetone and deionized water in order to remove the unreacted Al salt and porphyrin ligand. After drying, the as-made Al-PMOF was obtained as a reddish brown solid powder.

2.3. Synthesis of Al-PMOF (Fe), Al-PMOF (Co) and Al-PMOF (Cu)

For the synthesis of Al-PMOF(M), the facile post-synthetic method was adopted for the insertion of different substituted transition metals, including Fe, Co, and Cu into the porphyrin ring of Al-PMOF. The pre-activated Al-PMOF (100 mg, 0.11 mmol) was added into 25 mL of DMF and stirred for 10 min. Then, 2.2 mM cobalt acetate tetrahydrate was introduced into the above solution with constant stirring. The mixture was reacted with continuous stirring under 373 K in an oil bath for 48 h. After being cooled to room temperature, the sample was collected with filtration and washed successively with DMF, deionized water, and acetone. Finally, Al-PMOF(Co) was dried in a vacuum oven at 120 °C overnight. The synthetic process of Al-PMOF (Fe) and Al-PMOF (Cu) were similar to that of Al-PMOF(Co), except cobalt acetate tetrahydrate was replaced by ferrous acetate tetrahydrate, copper acetate monohydrate. Al-PMOF (Co) with different Co loading were synthesized by varying the concentration of cobalt, copper, and ferrous acetate salts.

2.4. Physical characterization

The crystalline structures of all films were identified by X-ray diffraction (XRD, D/Max2250, Rigaku) using Cu Kα radiation (λ = 0.15406 nm). The morphologies of the as-prepared composites were observed by a scanning electron microscope (SEM, JSM-7610FPlus). The energy dispersive X-ray spectroscopy (EDX) was used for elemental analyses with the accelerating voltage of 15 kV. The transmission electron microscopy (TEM) images were obtained by Model G2 F20 equipped with energy dispersive X-ray spectroscopy (EDS) mapping. Aberration-corrected high-angle annular dark-field scanning transmission electron microscopy (AC HAADF-STEM) was measured by FEI Themis Z. The surface composition and elemental valence state were examined by using an X-ray photoelectron spectrometer (XPS, K-Alpha 1063, Thermo Scientific), utilizing 50.00 eV pass energy. The band energies were calibrated with respect to the residual C 1 s peaks. The UV–vis absorption spectra were recorded through a diffuse reflectance-ultraviolet (DR-UV) spectrophotometer (TU-1901). FT-IR spectra were recorded on a Nicolet 6700 Fourier Transform Infrared Spectroscopy using KBr pellets. Inductively Coupled Plasma Mass Spectrometry (ICP-MS, Agilent 7700 s) was used to measure the content of metal atoms in the samples. *In situ* FTIR was carried out on a Nicolet iS50 FT-IR spectrometer equipped with an MCT detector cooled with liquid nitrogen. The Au-coated Si semi-cylindrical prism (20 mm in diameter) was used as the conductive substrate for catalysts and the IR refection element. The catalysts suspensions were dropped on the Au/Si surface as the

working electrode. The mass loading of the catalyst was 0.5 mg/cm^2 and the electrolyte was 0.1 M $KHCO_3$. *In situ* FTIR spectra were recorded during stepping the working electrode potential.

2.5. Photoelectrochemical measurements

All the photoelectrochemical (PEC) tests were carried out at room temperature by using an electrochemical workstation with a three-electrode configuration under simulated AM 1.5 G illumination (100 mW cm^{-2}). In this setup, the as-prepared samples, a platinum plate, an Ag/AgCl electrode, and 0.1 M $KHCO_3$ (pH = 6.8) were used as the working electrode, counter electrode, reference electrode, and electrolyte, respectively. The preparation of working electrode: 5 mg catalyst mixed with 5 mg Vulcan XC-72 were dispersed in 1 mL deionized water, 1 mL isopropanol and 50 μL Nafion (5 wt%) solution followed by sonication of 30 min to form a homogenic solution. The as-prepared catalyst ink was dropped onto a carbon paper (0.5 mg/cm^2) and dried at 60 °C overnight. All the as-prepared samples were illuminated from the front side. The photocurrent curve was obtained at a scanning rate of 20 mV/s. The electrochemical impedance spectroscopy (EIS) was carried out in different potentials with an AC frequency ranging from 10 kHz to 100 mHz and analyzed by Z-View program (Scribner Associates, Inc.). The PEC CO_2 reduction measurement was carried out in a gas-tight cell with two-compartments separated by a Nafion 117 membrane. The electrolyte in the cathode compartment was saturated with CO_2 by bubbling CO_2 gas for at least 30 min. Then, the gas phase products were collected by using Agilent 8860, equipped with a flame ionization detector and TCD. And the liquid phase products were analyzed using NMR (Avance III 600 MHz NMR, Bruker).

2.6. Computational methods

Gaussian 09 program package [34] was used to investigate the effect of light on catalytic activity. All structures were optimized at the PBE0 level of theory [35] with the def2-SVP basis set [36,37]. TD-DFT (time-dependent density functional theory) calculations were performed at the PBE0/def2-TZVP level. Then, Vienna Ab initio Simulation Package (VASP) [38] with the projector augmented wave (PAW) method [39] was also performed. The exchange-functional is treated using the generalized gradient approximation (GGA) of Perdew-Burke-Ernzerhof (PBE) functional [40]. The Spin-polarizations were carried out for all calculations. The energy cutoff for the plane wave basis expansion was set to 450 eV and the force on each atom less than 0.03 eV/Å was set for convergence criterion of geometry relaxation. The k-points in the Brillouin zone were sampled by a 2 × 2 × 1 grid. The self-consistent calculations apply a convergence energy threshold of 10^{-5} eV. The DFT-D3 method was employed to consider the van der Waals interaction [41]. The charge density isosurface level was set to 0.003 bohr^{-3}. Free energy diagrams for CO_2 reduction reaction were computed using a computational hydrogen electrode (CHE) model [42,43], which suggests that the chemical potential of a proton/electron ($H^+ + e^-$) is equal to half of that of one H_2 gas molecule. The free energies of the CO_2 reduction reaction steps were calculated by the equation [44]: $\Delta G = \Delta E_{DFT} + \Delta E_{ZPE} - T\Delta S$, where ΔE_{DFT} is the DFT electronic energy difference of each step, ΔE_{ZPE} and ΔS are the correction of zero-point energy and the variation of entropy, respectively, which are obtained by vibration analysis, and T is the temperature (T = 300 K).

3. Results and Discussion

3.1. Synthesis and characterization of materials

The parent Al-PMOF was prepared via a reported hydrothermal method with minor modification (see the Supporting Information) [26]. The preparation of Al-PMOF(Cu), Al-PMOF(Co) and Al-PMOF(Fe) was achieved by inserting transition metals (TMs) into Al-PMOF (Scheme 1). In the structure, Al is located in the octahedral sites, while transition metals (Cu, Co, Fe) are lied in porphyrin centres. Al-PMOF with Al-carboxylate coordination presents high chemical and thermal stability. Metalating the porphyrin units by Cu, Co, Fe can further modulate the electronic structure of Al-PMOF, thus improving photo-coupled electrochemical CO_2 reduction activity in aqueous solution. SEM images indicate that the parent Al-PMOF possesses the morphology of uniform nanoplate (Fig. S1a). Al-PMOF (Co), Al-PMOF (Cu) and Al-PMOF (Fe) also presents the similar morphology with Al-PMOF (Fig. S1b, Fig. S2), indicating that the insertion of TMs does not affect the morphology of Al-PMOF. Further observation of high-resolution SEM images verifies the nanoplate-like structure from Al-PMOF and Al-PMOF (Co) (Fig. 1a, b).

Similarly, TEM images also confirm that the Al-PMOF show a sheet-like morphology (Fig. S3). After inserting Co, the Al-PMOF (Co) still maintains the morphology of sheet (Fig. 1c and Fig. S4). Furthermore, the high-angle annular dark-field scanning TEM (HAADF-STEM) images also indicate that the morphology of Al-PMOF (Co) is well maintained after Co atoms implanted (Fig. 1d). No aggregated Co particles are detected, suggesting that Co species probably exist as mononuclear sites.

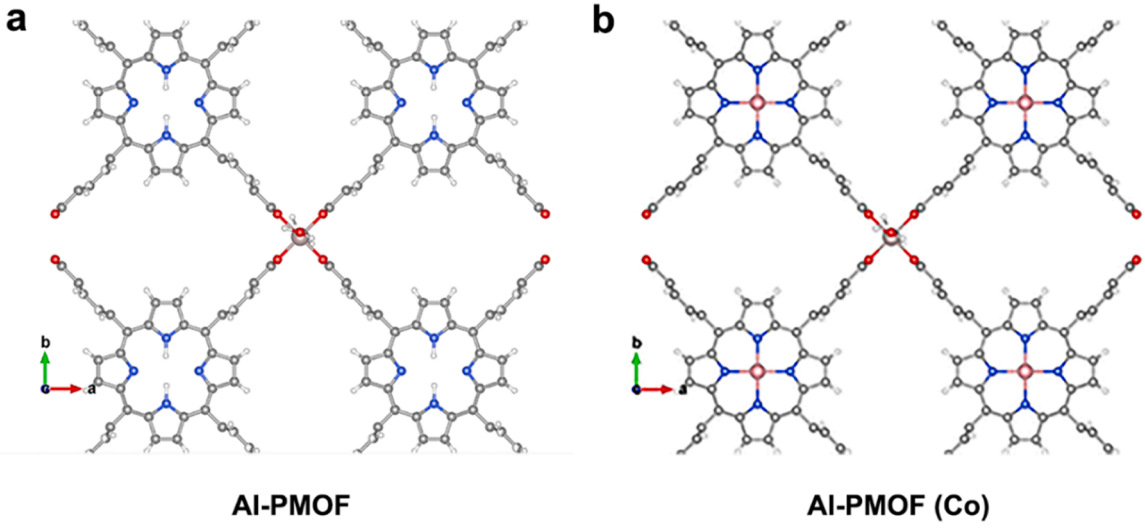

Scheme 1. Crystal structure of (a) Al-PMOF (C, dark grey; H, white; Al, light grey; O, red; N, blue); (b) Al-PMOF (Co) (C, dark grey; H, white; Co, pink; Al, light grey; O, red; N, blue).

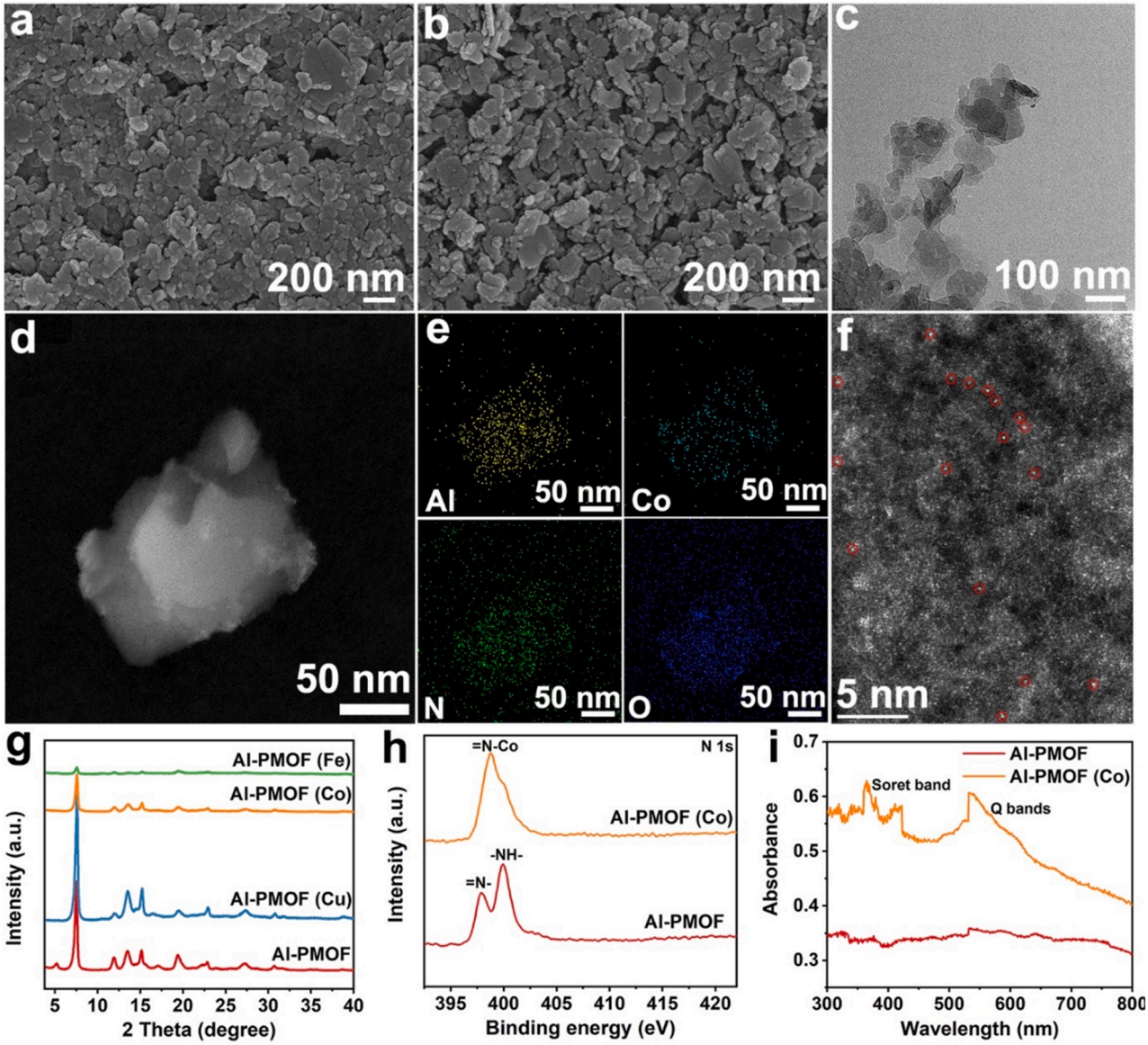

Fig. 1. The SEM images of (a) Al-PMOF, (b) Al-PMOF (Co); TEM images of (c) Al-PMOF (Co); HAADF-STEM and EDX elemental mapping images of (d, e) Al-PMOF (Co); (f) AC HAADF-STEM image of Al-PMOF (Co); (g) XRD patterns; (h) High-resolution XPS spectra of N 1 s of Al-PMOF and Al-PMOF (Co); (i) UV-Vis diffuse reflection spectra of Al-PMOF and Al-PMOF (Co).

EDS elemental mapping images indicate the homogeneous distribution of Co, C, N, O and Al elements in the entire skeleton of Al-PMOF (Co) without obvious aggregation (Fig. 1e; Fig. S5). Al-PMOF also exhibits similar elemental distribution except for the Co element (Fig. S6). To confirm the existence form of Co species in the Al porphyrin structure, AC HAADF-STEM was performed and the result reveals that the dispersed Co species in Al-PMOF are in atomic leve (Fig. 1f).

3.2. Structure and surface chemistry characterization

To investigate the structural characterizations of the prepared catalysts, XRD measurements were conducted, as shown in Fig. 1g. The XRD patterns first reveal the good crystallinity and high purity of Al-PMOF and Al-PMOF (M). Specially, for Al-PMOF, all diffraction peaks belong to an orthorhombic structure in Cmmm space group. The Rietveld refinement indicates the orthorhombic cell parameters of Al-PMOF (a = 31.978 Å, b = 6.5812 Å, c = 16.7405 Å), which agrees with previous reports [16,20,45]. After the insertion of TMs (Fe, Co, Cu), the crystallinity and integrity of Al-PMOF are not affected, also indirectly suggesting that the inserted Co atom should be introduced into the center of the porphyrin rings with full occupancy. The Al-PMOF (Co) with different Co atom loadings also presents the same framework structure with Al-PMOF (Fig. S7). Additionally, FT-IR spectra prove the presence of key functional groups of the Al-PMOF and Al-PMOF (M), implying that TMs insertion does not affect the Al-PMOF framework (Fig. S8).

The electronic properties of Al-PMOF and Al-PMOF (Co) were further studied by XPS measurements. The full XPS spectrum discloses the coexistence of Co, N, C, O, and Al elements (Fig. S9, Supporting information). As for XPS spectrum of N 1 s, there are two signals for Al-PMOF at 399.9 eV and 397.9 eV, which are assigned to −NH− and =N − , respectively [46]. For Al-PMOF (Co), only one bands located at 398.7 eV is observed, attributing to =N − Co (Fig. 1h). The phenomenon indicates that the introduction of Co into Al-PMOF coordinates with all the nitrogen atoms, in good agreement with the above discussion. In terms of Co element, two peaks located at ≈ 780.7 eV (Co $2p_{3/2}$) and 796.3 eV (Co $2p_{1/2}$) with accompanying corresponding satellite peaks (Fig. S10) are ascribed to Co^{2+} [47–49]. For Al and O elements, the binding

energies present some negative or positive shift compared with the pristine Al-PMOF, which mainly result from the resultant strong electronic interaction after insertion into Co atom (Fig. S11). The scanned C 1 s spectrum (Fig. S12) can be deconvoluted into the following peaks (C═C, C═O, and O– C═O) [50,51].

The ultraviolet−visible (UV−vis) absorption spectra show strong absorption in the range of 300–800 nm, which is attributed to the presence of porphyrin units with photosensitivity [52]. It is found that Al-PMOF (Co) exhibits higher visible light absorption (Fig. 1i). Note that the number of Q bands (500–700 nm) decreases to two for Al-PMOF (Co) from four for Al-PMOF (Fig. S13a), implying an increase in symmetry after Co insertion [16,46]. Similarly, the UV–vis absorption spectra of Al-PMOF (Fe) and Al-PMOF (Cu) also present the same result (Fig. S13b). Tauc plots indicate that the HOMO–LUMO gap decreases with the introduction of Co (Fig. S14), which is consistent with the previous report [8]. These results display that Al-PMOF and Al-PMOF (Co) can regard as good photon absorbers and excite electron–hole pairs under light condition.

3.3. Photo-coupled electrochemical CO_2 reduction performance

To shed light on the photo-coupled electrochemical CO_2 reduction performance of Al-PMOF (Co), photo-coupled electrochemical tests were carried out in a H-cell with a CO_2-saturated 0.1 M $KHCO_3$ electrolyte (pH = 6.8) (Fig. S15). From the result of the linear sweep voltammetry curves, the current densities of Al-PMOF (M) are much larger than those of Al-PMOF (Fig. S16a), indicating that the incorporation of M into Al-PMOF effectively accelerates charge transfer. And Al-PMOF (Co) possesses an increased current density from − 9.1 to − 10.0 mA/cm^2 at − 1.2 V vs. RHE in the presence of illumination (Fig. 2a), suggesting that the introduction of Co can assist porphyrin units to transfer more electrons under light condition. Simultaneously, it is found that Al-

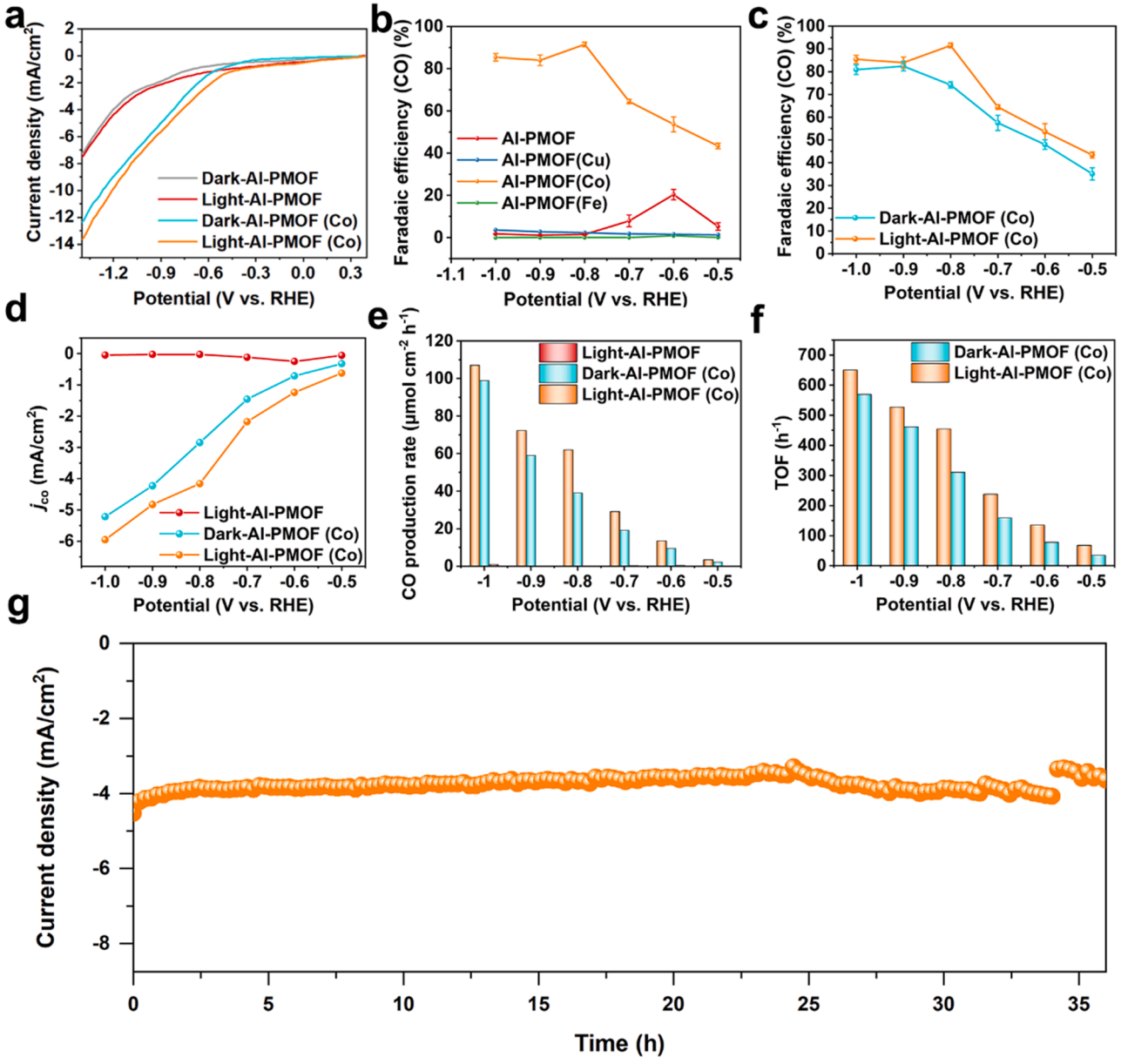

Fig. 2. Evaluation of photo-coupled electrochemical CO_2 reduction performance of Al-PMOF and Al-PMOF (Co) by photo-coupled electrochemical measurements. (a) LSV curves of Al-PMOF and Al-PMOF (Co) in CO_2-saturated 0.1 m $KHCO_3$ solution under dark and light condition; (b) FE_{CO} of Al-PMOF and Al-PMOF (M) under visible light; (c) FE_{CO} of Al-PMOF (Co) under dark and light condition; The CO (d) current density j_{CO} and (e) production rate of Al-PMOF and Al-PMOF (Co) under dark and light condition; (f) TOF of Al-PMOF (Co) under dark and light condition; (g) The stability test of Al-PMOF (Co) at − 0.8 V vs. RHE under visible light.

PMOF (Co) samples exhibit higher current densities with the augment of concentration of cobalt salt (Fig. S16b), implying that Co atoms could be active sites for CO_2 reduction. Moreover, the Al-PMOF (Co) achieves a maximum Faradaic efficiency (FE) for CO production of ~90% at − 0.8 V vs. RHE under visible light without other liquid products, compared with Al-PMOF, Al-PMOF (Fe) and Al-PMOF (Cu) (Fig. 2b, Fig. S17-S18), which could be attributed to the better affinity of unsaturated Co sites toward CO_2.

Encouragingly, the FE of CO of Al-PMOF (Co) exhibits obvious improvement over a wide potential range from − 0.5 V vs. RHE to − 1.0 V vs. RHE under visible light, which is higher than that measured under dark conditions (Fig. 2c). This result further verifies that photo-driven porphyrin can mitigate more electrons. The CO current density (j_{CO}) can be obtained under different potentials according the data of current density in combination with FE_{CO}. As revealed by j_{CO} (Fig. 2d), Al-PMOF (Co) gives rise to a j_{CO} of − 5.95 mA/cm^2 at − 1.0 V vs. RHE under visible light, which exceeds that of Al-PMOF and that measured under dark. To further assess the synergistic effect of the inserted Co site and external light-field on the CO_2 reduction performance, the CO production rate was determined and shown in Fig. 2e. Compared with Al-PMOF, as expected, the CO production rate is significantly enhanced at more negative potentials. Especially when introducing additional light-field, the CO production rate rises up to 107.1 μmmol cm^{-2} h^{-1} at − 1.0 V vs. RHE. The improved CO_2 reduction performance demonstrates once again that external light-field is conducive to promote electron transfer ability of Al-PMOF (Co). The larger current densities of Al-PMOF (Fe) and Al-PMOF (Cu) under light condition than those under dark condition also verified the positive effect of light-field (Fig. S19). Additionally, a series of Al-PMOF (Co) catalysts with different Co concentrations were synthesized to further explore the effect of Co site on CO_2 reduction performance (Fig. S20). For varying Co concentration, the FE_{CO} change slightly as Co content increase (Fig. S21).

Remarkably, Al-PMOF (Co) displays a larger TOF value of 650 h^{-1} at − 1.0 V vs. RHE under visible-light, which surpass the value that measured under dark (Fig. 2 f). Thus, the result of TOF further manifests that more photo-generated electrons are involved into CO_2 reduction under visible light. In addition to the above activity and selectivity, the durability of Al-PMOF and Al-PMOF (Co) was explored at − 0.8 V vs.

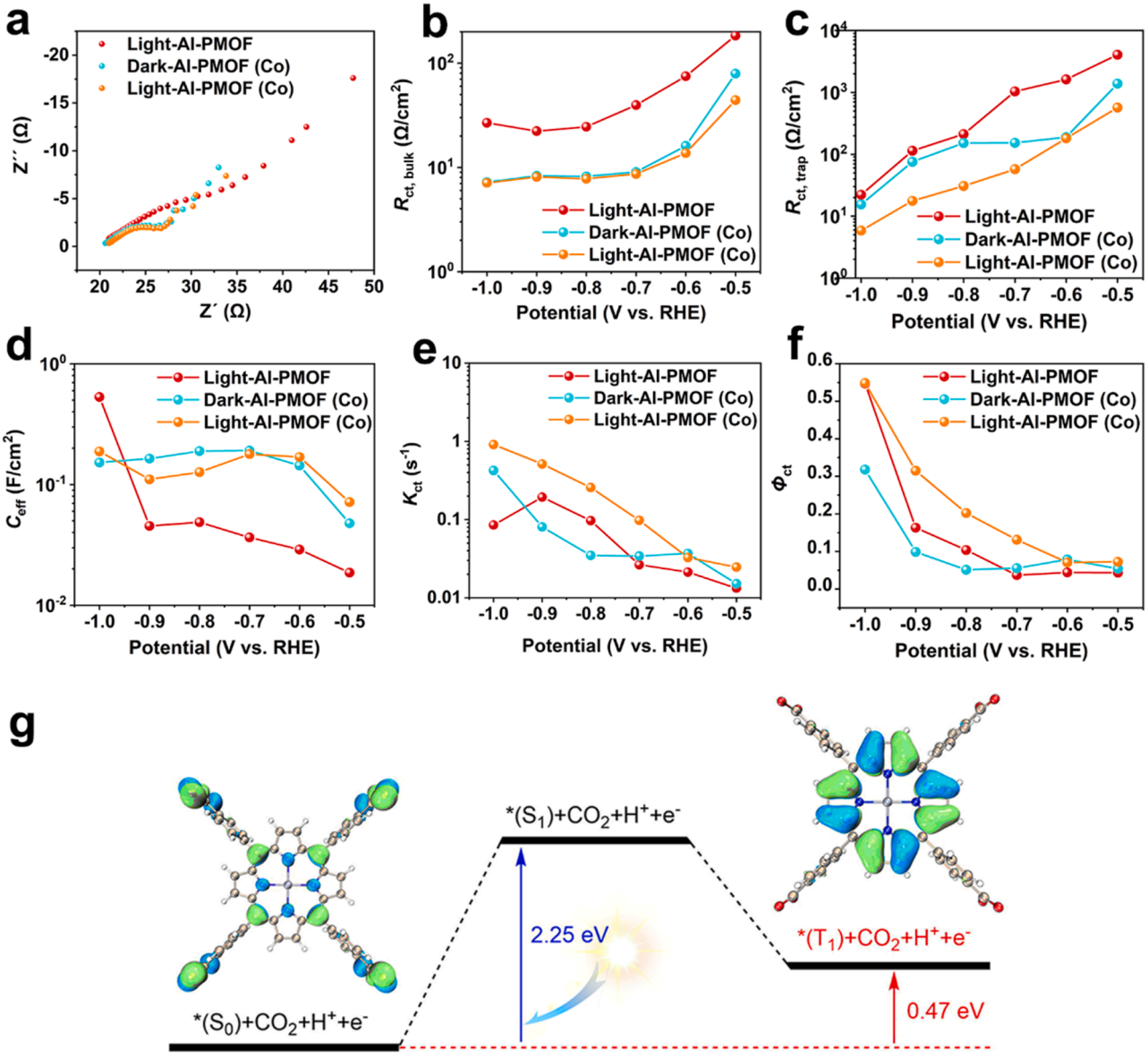

Fig. 3. (a) EIS spectra measured at − 0.8 V vs. RHE; (b-d) Fitting results from EIS measurements at different potential; (e) Charge transfer (K_{ct}) rate; (f) Calculated charge transfer efficiency (Φ_{ct}) of Al-PMOF and Al-PMOF (Co); (g) Schematic representation of the excited states of Al-PMOF (Co).

RHE under light condition. As expected, in comparison with Al-PMOF, the higher current density of Al-PMOF(Co) presents almost constant over 35 h photo-coupled electrochemical CO_2 reduction. And the corresponding FE_{CO} also show slightly degradation under same condition (Fig. 2 g, Fig. S22-S23), proving that Al-PMOF (Co) can maintain satisfactory long-term stability during photo-coupled electrochemical CO_2 reduction. The SEM images after stability test also further confirm the good stability of Al-PMOF (Co) (Fig. S24). Besides, the XPS results recorded before and after stability test show that the elements in the catalyst could be well maintained (Fig. S25).

3.4. Photo-coupled electrocatalytic behavior

To gain a deep insight into the photo-coupled electrocatalytic mechanism, EIS and PEIS measurements are performed to research the charge transfer process over Al-PMOF and Al-PMOF (Co) during photo-coupled electrochemical CO_2 reduction. As shown in Fig. 3a, there are two semicircles, located at high frequency (HF) and low frequency (LF), respectively. Thereinto, the semicircle at HF is in connection with the charge transfer resistance in bulk catalyst, while the semicircle at LF is associated with the charge transfer resistance at the catalyst/electrolyte interface [53,54]. In comparison with Al-PMOF, Al-PMOF (Co) exhibits the smaller semicircle in the region of HF and LF under dark and light condition, meaning that Co implanted catalyst can promote charge separation and transfer. Meanwhile, it is noted that both Al-PMOF (Co) under dark and light condition shown similar semicircle at HF. In the region of LF, light-Al-PMOF (Co) possesses a smaller semicircle than dark-Al-PMOF. These phenomena indicate that visible light can accelerate charge transfer across the catalyst/electrolyte interface.

In order to certify the above conclusion, the equivalent circuit is employed for fitting the results of EIS and PEIS measurements [55] (Fig. S26). In this case, R_s (the solution resistance) are almost the same for Al-PMOF and Al-PMOF (Co) (Fig. S27). For $R_{ct,bulk}$ (bulk charge resistance), a dramatically decrease over Al-PMOF (Co) and a comparable value for light-Al-PMOF (Co) and dark- Al-PMOF (Co) is observed (Fig. 3b). Meanwhile, Al-PMOF (Co) also has smaller $R_{ct,trap}$ value compared with Al-PMOF and dark-Al-PMOF (Co), further suggesting that Co insertion can facilitate the bulk and surface charge transportation, while external light irradiation can further improve the interface electron transfer efficiency (Fig. 3c). The effective capacitance (C_{eff}) is also calculated and it is found that Al-PMOF (Co) have larger C_{eff} values (Fig. 3d), which may be interpreted as electron storage. This would mean that more electrons arrive on the surface of Al-PMOF (Co).

In general, it is well accepted that charge transfer and surface recombination exist near an electrode surface during CO_2 reduction reaction. According to the phenomenological model [53], the corresponding rate parameters are defined as the charge-transfer rate (K_{ct}) and surface recombination rate constant (K_{rec}), respectively. K_{ct} and K_{rec} can be calculated by the equations (See in the Supporting information). From the result of K_{ct}, light-Al-PMOF (Co) exhibits higher charge transfer rate than dark-Al-PMOF (Co) and Al-PMOF (Fig. 3e). This would further verify the conclusion for expediting charge transfer upon Co insertion and visible light introduction. Notice that a slight change in the K_{rec} is observed over Al-PMOF (Co) (Fig. S28). Charge transfer efficiency (Φ_{ct}) is of utmost importance for evaluating the photo-coupled electrocatalytic performance, which can be acquired through K_{ct} and K_{rec} in combination (See in the supporting formation). As revealed in Fig. 3f, a much higher Φ_{ct} is achieved even though a slight change in K_{rec} for Al-PMOF (Co), indicating that the Co incorporation can promote electron transfer from porphyrin units to Co-N site and visible light further improve efficiency in surface CO_2 reaction.

To further illustrate the effect of light on catalytic activity, the electronic properties of S_1 and T_1 excited states of Al-PMOF (Co) catalyst were calculated by Gaussian 09 program package. When external light field is introduced, Al-PMOF (Co) is first excited from the S_0 ground state to the S_1 excited state and return into the T_1 state through the intersystem crossing process (Fig. 3g). The S_1 and T_1 exited states of the Al-PMOF(Co) catalyst promote the electron-flow and CO_2 activation on Co site because of the ligand-to-metal charge transfer excitation characteristic. The photo-coupled electrocatalysis of CO_2 occurs mainly on the T_1 state of Al-PMOF (Co) instead of the S_0 state. Additionally, the energy required for T_1 state derives from the light absorption without electricity. Al-PMOF (Co) generates a higher energy excited state (1.2 eV vs. ground state) under light condition, indicating that light accelerates the electron transfer from the ligand to the active center.

3.5. Surface CO_2 reaction behavior

To explore the reaction mechanisms between the intermediates and catalyst surfaces, *in situ* FTIR was conducted and the corresponding spectra are shown in Fig. 4. Note that no other new infrared peaks are observed for Al-PMOF (Fig. 4a), implying that activating CO_2 is difficult. On the contrary, a new infrared peak at 1594 cm^{-1} and a peak at 1219 cm^{-1} for Al-PMOF (Co) under light and dark condition are found (Figs. 4b-4c), which are assigned to the characteristic peaks of the COOH* and HCO_3* group [56–58]. The COOH* group is generally perceived as the vital intermediate for producing CO during CO_2 reduction, while HCO_3* group results from the effect of bicarbonate in the electrolyte [59,60].

Most importantly, as shown in Fig. 4d, the in situ FTIR difference spectra of Al-PMOF (Co) under illumination and dark exhibits obvious signal of adsorption band of the intermediates, demonstrating that Al-PMOF (Co) can generate more COOH* groups with the existence of illumination. The above phenomenon means that the COOH* group could only be detected during CO_2 reduction process using Al-PMOF (Co), demonstrating that the COOH* intermediate can be generated on the Co site [61,62]. Then, the COOH* intermediate is rapidly protonated to produce CO*, which is desorbed from the surface of Al-PMOF (Co) to generate CO molecules. Correspondingly, the most possible reaction pathway for the catalytic system is shown below:

$$* + CO_2 + e^- + H^+ = COOH*$$

$$COOH* + e^- + H^+ = CO* + H_2O$$

$$CO* + e^- + H^+ = CO + *$$

in which * represents the active site. At the same time, the light-induced deviation in the *in situ* FTIR spectra indicates that an external light field can promote charge transfer for generating more COOH* intermediates. These results indicate that the introduction of atomic Co site and light field can promote the adsorption of the COOH* intermediate, thus making for producing CO molecules.

To further investigate surface CO_2 reaction mechanism, density functional theory (DFT) calculations on Al-PMOF and Al-PMOF (Co) were carried out, respectively (Methods in the Supporting information). The corresponding models were selected for calculations (Fig. S29). Then, each of the reaction intermediates (*CO_2, *COOH and *CO) absorbed on Al-PMOF and Al-PMOF (Co) was considered and optimized (Fig. S30). The reaction pathway free energies were calculated to explore the adsorption of *CO_2, *COOH and *CO intermediates on Al-PMOF and Al-PMOF (Co), as presented in Fig. 5a. Compared to Al-PMOF (- 0.15 eV), the Al-PMOF (Co) model exhibits lower *CO_2 adsorption energies of - 0.4 eV, suggesting its stronger *CO_2 adsorption capability for the subsequent CO_2 reduction into CO. When the absorbed CO_2 is converted to *COOH, the adsorption energy of Al-PMOF (Co) is 0.37 eV. In contrast, for Al-PMOF, the *COOH adsorption energy is + 2.07 eV, with a corresponding energy barrier as 2.22 eV, indicating that it is difficult to realize the reaction from *CO_2 to *COOH. Therefore, the Co-N site in Al-PMOF (Co) is more favorable for the following CO_2 reduction.

Given that the introduction of cobalt atom is of paramount important during CO_2 reduction, it is necessary to investigate the detailed orbital

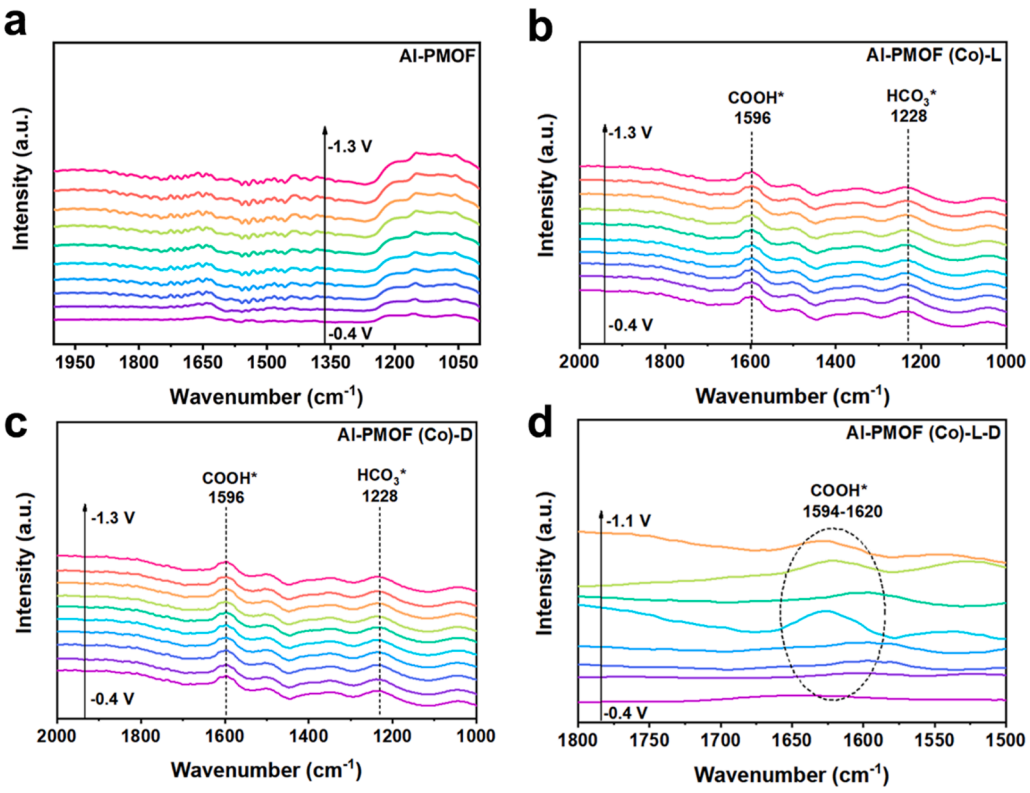

Fig. 4. *In situ* FTIR spectra of (a) Al-PMOF; Al-PMOF (Co) under (b) illumination and (c) dark; (d) The *in situ* FTIR difference spectra of Al-PMOF (Co) under illumination and dark.

information of the active cobalt center. As is clarified from the projected density of states (PDOS) analysis, it can be found that Al-PMOF (Co) shows a stronger bonding between Co sites and *COOH than Al-PMOF (Fig. 5b, d). Because the Co $3d_z^2$ orbital exist a large resonance with the 2p orbital of *COOH. Furthermore, previous research manifested that a large resonance between different orbitals at the same energy region implies a strong hybridization [47,63]. Similarly, PDOS of Al-PMOF (Co) has also a strong interaction with *CO compared with Al-PMOF (Fig. 5c, e). These results demonstrate that incorporating Co into Al-PMOF can facilitate the CO_2 activation and the following CO_2 reduction. In addition, it can also observe that the d_z^2 orbital of Al-PMOF (Co) before absorbed *COOH and *CO intermediates is closer to the Fermi level, further confirming the strong interactions of Co 3d orbitals and intermediates (*COOH and *CO) (Fig. S31-S32).

The electron structure difference of the Co active site is also of utmost importance for understanding the catalytic mechanism. The charge density differences and Bader charge analyses display that charge transfer from Al-PMOF (Co) to $*CO_2$, *COOH and *CO are 0.225 *e*, 0.639 *e* and 0.367 *e*, respectively, which are higher than those from Al-PMOF (0.196 *e*, 0.521 *e* and 0.239 *e*) (Fig. 5f), suggesting the stronger combination with Co site and the intermediates ($*CO_2$, *COOH, *CO). These results are consistent with those of PDOS (Fig. S33-34). Besides, the introduction of Co atom shows density of states on the fermi level so that the electrical conductivity of Al-PMOF is boosted greatly (Fig. S35). As a consequence, inserting Co atom into porphyrin unit exhibits superior performance in CO_2 activation.

4. Conclusion

In summary, we have successfully developed a meaningful Al-based porphyrinic metal-organic framework (Al-PMOF) with different metal centers (Fe, Co, Cu) as CO_2 reduction photo-coupled electrocatalysts for CO_2 reduction in aqueous solution for the first time. Benefitting from high-stability Al-oxo chain and good reduction activity of Co site, the Al-PMOF (Co) achieves a high Faradaic efficiency of ~90% in CO generation under visible light. More importantly, a long-term stability without performance decay is obtained on Al-PMOF (Co). The introduction of Co site into Al-PMOF modulates electronic nature of d-states, optimizing the adsorption of CO_2, intermediate *COOH and *CO, which is more favorable for the following CO_2 reduction. Furthermore, incorporating Co sites makes $3d_z^2$ orbital exist a large resonance with the 2p orbital of *COOH intermediate, thus inducing CO_2 reduction though a favorable pathway. From the view of charge transfer mechanism, Co insertion expedites charge transfer rate (K_{ct}) and visible light accelerates charge transfer, and consequently the charge transfer efficiency (Φ_{ct}) is improved. The study sheds new light on enhancing CO_2 reduction performance by tuning the active site and introducing external light field.

CRediT authorship contribution statement

Keke Wang: Methodology, Visualization, Investigation, Data curation, Writing – original draft. **Yang Liu:** Calculation, Methodology. **Jihu Kang:** Methodology, Visualization, Investigation. **Yanfang Zhang:** Investigation, Validation. **Qingmei Wang:** Investigation. **Long Chen:** Investigation. **Qiyou Wang:** Measurements. **Bao Liu:** Measurements. **Min Liu:** Writing – review & editing, Supervision. **Xiaoqing Qiu:** Writing – review & editing, Supervision. **Wenzhang Li:** Supervision, Conceptualization, Writing – review & editing. **Jie Li:** Supervision, Conceptualization, Writing – review & editing.

Declaration of Competing Interest

The authors declare that they have no known competing financial interests or personal relationships that could have appeared to influence the work reported in this paper.

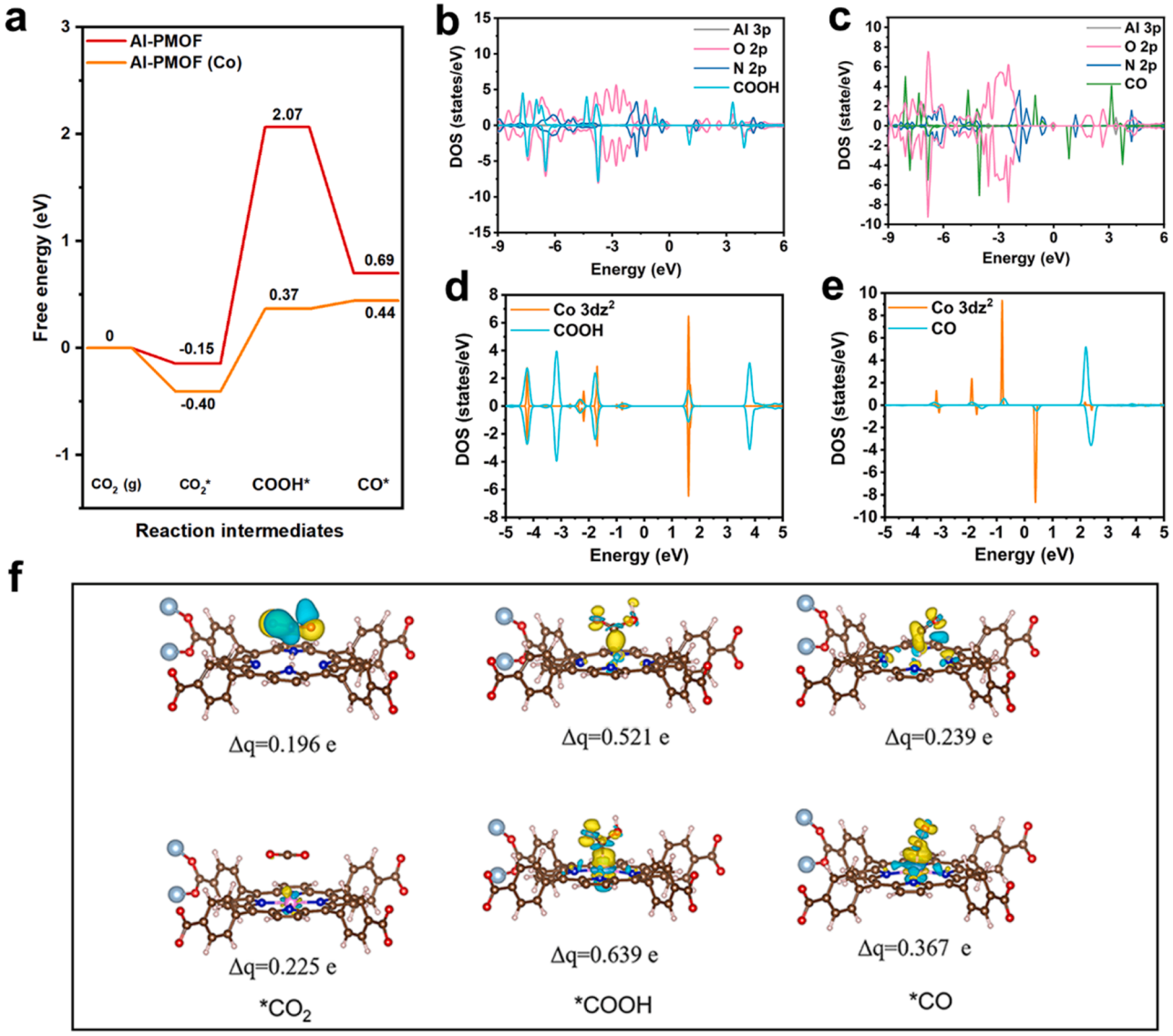

Fig. 5. (a) Free energy diagram of Al-PMOF and Al-PMOF(Co); (b-c) PDOS for *COOH (b) and *CO (c) adsorbed on Al-PMOF; (d-e) PDOS for *COOH (d) and *CO (e) adsorbed on Al-PMOF (Co); (f) The charge density differences and Bader charge transfer for CO_2; *CO and *COOH intermediates adsorbed on Al-PMOF and Al-PMOF (Co).

Data Availability

Data will be made available on request.

Acknowledgements

This study was supported by the National Natural Science Foundation of China (22078368), and the Hunan Provincial Science and Technology Plan Project of China (no. 2017TP1001). We are grateful for resources from the High Performance Computing Center of Central South University.

Appendix A. Supporting information

Supplementary data associated with this article can be found in the online version at doi:10.1016/j.apcatb.2022.122315.

References

[1] S. Zhu, X. Li, X. Jiao, W. Shao, L. Li, X. Zu, J. Hu, J. Zhu, W. Yan, C. Wang, Y. Sun, Y. Xie, Selective CO_2 photoreduction into C_2 product enabled by charge-polarized metal pair sites, Nano Lett. 21 (2021) 2324–2331.
[2] P. Iyengar, M.J. Kolb, J.R. Pankhurst, F. Calle-Vallejo, R. Buonsanti, Elucidating the facet-dependent selectivity for CO_2 electroreduction to ethanol of Cu–Ag tandem catalysts, ACS Catal. 11 (2021) 4456–4463.
[3] G.W. Woyessa, B. Jay-ar, M. Rameez, C.-H. Hung, Nanocomposite catalyst of graphitic carbon nitride and Cu/Fe mixed metal oxide for electrochemical CO_2 reduction to CO, Appl. Catal. B Environ. 291 (2021) 120052–120061.
[4] S. Lin, C.S. Diercks, Y.-B. Zhang, N. Kornienko, E.M. Nichols, Y. Zhao, A.R. Paris, D. Kim, P. Yang, O.M. Yaghi, Covalent organic frameworks comprising cobalt porphyrins for catalytic CO_2 reduction in water, Science 349 (2015) 1208–1213.
[5] L. Zhang, Z.-J. Zhao, T. Wang, J. Gong, Nano-designed semiconductors for electro- and photoelectro-catalytic conversion of carbon dioxide, Chem. Soc. Rev. 47 (2018) 5423–5443.
[6] Z. Li, R. Wu, L. Zhao, P. Li, X. Wei, J. Wang, J.S. Chen, T. Zhang, Metal-support interactions in designing noble metal-based catalysts for electrochemical CO_2 reduction: recent advances and future perspectives, Nano Res. 14 (2021) 3795–3809.
[7] X. Huang, Q. Shen, J. Liu, N. Yang, G. Zhao, A CO_2 adsorption-enhanced semiconductor/metal-complex hybrid photoelectrocatalytic interface for efficient formate production, Energy Environ. Sci. 9 (2016) 3161–3171.

[8] D. Yang, H. Yu, T. He, S. Zuo, X. Liu, H. Yang, B. Ni, H. Li, L. Gu, D. Wang, X. Wang, Visible-light-switched electron transfer over single porphyrin-metal atom center for highly selective electroreduction of carbon dioxide, Nat. Commun. 10 (2019) 1–10.

[9] X. Xiong, Y. Zhao, R. Shi, W. Yin, Y. Zhao, G.I. Waterhouse, T. Zhang, Selective photocatalytic CO_2 reduction over Zn-based layered double hydroxides containing tri or tetravalent metals, Sci. Bull. 65 (2020) 987–994.

[10] J. Qin, S. Wang, X. Wang, Visible-light reduction CO_2 with dodecahedral zeolitic imidazolate framework ZIF-67 as an efficient co-catalyst, Appl. Catal. B Environ. 209 (2017) 476–482.

[11] K. Wang, Y. Ma, Y. Liu, W. Qiu, Q. Wang, X. Yang, M. Liu, X. Qiu, W. Li, J. Li, Insights into the development of Cu-based photocathodes for carbon dioxide (CO_2) conversion, Green. Chem. 23 (2021) 3207–3240.

[12] X. Deng, R. Li, S. Wu, L. Wang, J. Hu, J. Ma, W. Jiang, N. Zhang, X. Zheng, C. Gao, L. Wang, Q. Zhang, J. Zhu, Y. Xiong, Metal-organic framework coating enhances the performance of Cu_2O in photoelectrochemical CO_2 reduction, J. Am. Chem. Soc. 141 (2019) 10924–10929.

[13] M.E. Aguirre, R. Zhou, A.J. Eugene, M.I. Guzman, M.A. Grela, Cu_2O/TiO_2 heterostructures for CO_2 reduction through a direct Z-scheme: protecting Cu_2O from photocorrosion, Appl. Catal. B Environ. 217 (2017) 485–493.

[14] G. Liu, F. Zheng, J. Li, G. Zeng, Y. Ye, D.M. Larson, J. Yano, E.J. Crumlin, J. W. Ager, L.-w Wang, F.M. Toma, Investigation and mitigation of degradation mechanisms in Cu_2O photoelectrodes for CO_2 reduction to ethylene, Nat. Energy 6 (2021) 1124–1132.

[15] D.G. Johnson, M.P. Niemczyk, D.W. Minsek, G.P. Wiederrecht, W.A. Svec, G. L. Gaines III, M.R. Wasielewski, Photochemical electron transfer in chlorophyll-porphyrin-quinone triads: the role of the porphyrin-bridging molecule, , J. Am. Chem. Soc. 115 (1993) 5692–5701.

[16] S. Shang, W. Xiong, C. Yang, B. Johannessen, R. Liu, H.Y. Hsu, Q. Gu, M.K. H. Leung, J. Shang, Atomically dispersed iron metal site in a porphyrin-based metal-organic framework for photocatalytic nitrogen fixation, ACS nano 15 (2021) 9670–9678.

[17] J. Liu, H. Shi, Q. Shen, C. Guo, G. Zhao, A biomimetic photoelectrocatalyst of Co–porphyrin combined with a g-C_3N_4 nanosheet based on π–π supramolecular interaction for high-efficiency CO_2 reduction in water medium, Green. Chem. 19 (2017) 5900–5910.

[18] T. Wang, L. Xu, Z. Chen, L. Guo, Y. Zhang, R. Li, T. Peng, Central site regulation of cobalt porphyrin conjugated polymer to give highly active and selective CO_2 reduction to CO in aqueous solution, Appl. Catal. B Environ. 291 (2021) 120128–120138.

[19] S. Xie, Y. Li, B. Sheng, W. Zhang, W. Wang, C. Chen, J. Li, H. Sheng, J. Zhao, Self-reconstruction of paddle-wheel copper-node to facilitate the photocatalytic CO_2 reduction to ethane, Appl. Catal. B Environ. 310 (2022) 121320–121329.

[20] A. Fateeva, P.A. Chater, C.P. Ireland, A.A. Tahir, Y.Z. Khimyak, P.V. Wiper, J. R. Darwent, M.J. Rosseinsky, A water-stable porphyrin-based metal–organic framework active for visible-light photocatalysis, Angew. Chem. Int. Ed. 51 (2012) 7440–7444.

[21] J.-L. Wang, C. Wang, W. Lin, Metal–organic frameworks for light harvesting and photocatalysis, ACS Catal. 2 (2012) 2630–2640.

[22] J.H. Cavka, S. Jakobsen, U. Olsbye, N. Guillou, C. Lamberti, S. Bordiga, K. P. Lillerud, A new zirconium inorganic building brick forming metal organic frameworks with exceptional stability, J. Am. Chem. Soc. 130 (2008) 13850–13851.

[23] I.J. Kang, N.A. Khan, E. Haque, S.H. Jhung, Chemical and thermal stability of isotypic metal–organic frameworks: effect of metal ions, Chem. Eur. J. 17 (2011) 6437–6442.

[24] M. Kandiah, M.H. Nilsen, S. Usseglio, S. Jakobsen, U. Olsbye, M. Tilset, C. Larabi, E.A. Quadrelli, F. Bonino, K.P. Lillerud, Synthesis and stability of tagged UiO-66 Zr-MOFs, Chem. Mater. 22 (2010) 6632–6640.

[25] T. Loiseau, C. Serre, C. Huguenard, G. Fink, F. Taulelle, M. Henry, T. Bataille, G. Férey, A rationale for the large breathing of the porous aluminum terephthalate (MIL-53) upon hydration, Chem. Eur. J. 10 (2004) 1373–1382.

[26] P.G. Boyd, A. Chidambaram, E. Garcia-Diez, C.P. Ireland, T.D. Daff, R. Bounds, A. Gladysiak, P. Schouwink, S.M. Moosavi, M.M. Maroto-Valer, J.A. Reimer, J.A. R. Navarro, T.K. Woo, S. Garcia, K.C. Stylianou, B. Smit, Data-driven design of metal-organic frameworks for wet flue gas CO_2 capture, Nature 576 (2019) 253–256.

[27] F. Li, G.-F. Han, J.-B. Baek, Active site engineering in transition metal based electrocatalysts for green energy applications, Acc. Mater. Res. 2 (2021) 147–158.

[28] J. Low, J. Ma, J. Wan, W. Jiang, Y. Xiong, Identification and design of active sites on photocatalysts for the direct artificial carbon cycle, Acc. Mater. Res. 3 (2021) 331–342.

[29] Z. Zeng, L.Y. Gan, H. Bin Yang, X. Su, J. Gao, W. Liu, H. Matsumoto, J. Gong, J. Zhang, W. Cai, Z. Zhang, Y. Yan, B. Liu, P. Chen, Orbital coupling of hetero-diatomic nickel-iron site for bifunctional electrocatalysis of CO_2 reduction and oxygen evolution, Nat. Commun. 12 (2021) 1–11.

[30] Q. Yin, E.V. Alexandrov, D.H. Si, Q.Q. Huang, Z.B. Fang, Y. Zhang, A.A. Zhang, W. K. Qin, Y.L. Li, T.F. Liu, D.M. Proserpio, Metallization-prompted robust porphyrin-based hydrogen-bonded organic frameworks for photocatalytic CO_2 reduction, Angew. Chem. 61 (2022) e202115854.

[31] Y. Zhou, L. Zheng, D. Yang, H. Yang, Q. Lu, Q. Zhang, L. Gu, X. Wang, Enhancing CO_2 electrocatalysis on 2D porphyrin-based metal–organic framework nanosheets coupled with visible-light, Small Methods 5 (2020) 2000991–2000998.

[32] S.S. Wang, H.H. Huang, M. Liu, S. Yao, S. Guo, J.W. Wang, Z.M. Zhang, T.B. Lu, Encapsulation of single iron sites in a metal-porphyrin framework for high-performance photocatalytic CO_2 reduction, Inorg. Chem. 59 (2020) 6301–6307.

[33] Y.-R. Wang, Q. Huang, C.-T. He, Y. Chen, J. Liu, F.-C. Shen, Y.-Q. Lan, Oriented electron transmission in polyoxometalate-metalloporphyrin organic framework for highly selective electroreduction of CO_2, Nat. Commun. 9 (2018) 1–8.

[34] R.A. Gaussian09, 1, mj frisch, gw trucks, hb schlegel, ge scuseria, ma robb, jr cheeseman, g. Scalmani, v. Barone, b. Mennucci, ga petersson et al., gaussian, Inc., Wallingford CT, 121 (2009) 150–166.

[35] C. Adamo, V. Barone, Toward reliable density functional methods without adjustable parameters: the PBE0 model, J. Chem. Phys. 110 (1999) 6158–6170.

[36] F. Weigend, R. Ahlrichs, Balanced basis sets of split valence, triple zeta valence and quadruple zeta valence quality for H to Rn: design and assessment of accuracy, Phys. Chem. Chem. Phys. 7 (2005) 3297–3305.

[37] F. Weigend, Accurate coulomb-fitting basis sets for H to Rn, Phys. Chem. Chem. Phys. 8 (2006) 1057–1065.

[38] G. Kresse, J. Furthmüller, Efficiency of ab-initio total energy calculations for metals and semiconductors using a plane-wave basis set, Comp, Mater. Sci. 6 (1996) 15–50.

[39] P.E. Blöchl, Projector augmented-wave method, Phys. Rev. B 50 (1994) 17953.

[40] J.P. Perdew, J.A. Chevary, S.H. Vosko, K.A. Jackson, M.R. Pederson, D.J. Singh, C. Fiolhais, Atoms, molecules, solids, and surfaces: applications of the generalized gradient approximation for exchange and correlation, Phys. Rev. B 46 (1992) 6671–6687.

[41] S. Grimme, J. Antony, S. Ehrlich, H. Krieg, A consistent and accurate ab initio parametrization of density functional dispersion correction (DFT-D) for the 94 elements H-Pu, J. Chem. Phys. 132 (2010) 154104–154122.

[42] V. Viswanathan, H.A. Hansen, J. Rossmeisl, J.K. Nørskov, Unifying the $2e^-$ and $4e^-$ reduction of oxygen on metal surfaces, J. Phys. Chem. Lett. 3 (2012) 2948–2951.

[43] H.-Y. Su, Y. Gorlin, I.C. Man, F. Calle-Vallejo, J.K. Nørskov, T.F. Jaramillo, J. Rossmeisl, Identifying active surface phases for metal oxide electrocatalysts: a study of manganese oxide Bi-functional catalysts for oxygen reduction and water oxidation catalysis, Phys. Chem. Chem. Phys. 14 (2012) 14010–14022.

[44] E. Skulason, T. Bligaard, S. Gudmundsdóttir, F. Studt, J. Rossmeisl, F. Abild-Pedersen, T. Vegge, H. Jónsson, J.K. Nørskov, A theoretical evaluation of possible transition metal electro-catalysts for N_2 reduction, Phys. Chem. Chem. Phys. 14 (2012) 1235–1245.

[45] X. Gong, Y. Shu, Z. Jiang, L. Lu, X. Xu, C. Wang, H. Deng, Metal–organic frameworks for the exploitation of distance between active sites in efficient photocatalysis, Angew. Chem. 132 (2020) 5364–5369.

[46] Y. Liu, Y. Yang, Q. Sun, Z. Wang, B. Huang, Y. Dai, X. Qin, X. Zhang, Chemical adsorption enhanced CO_2 capture and photoreduction over a copper porphyrin based metal organic framework, ACS Appl. Mater. Interfaces 5 (2013) 7654–7658.

[47] Z. Zhang, J. Xiao, X.J. Chen, S. Yu, L. Yu, R. Si, Y. Wang, S. Wang, X. Meng, Y. Wang, Reaction mechanisms of well-defined metal–N_4 sites in electrocatalytic CO_2 reduction, Angew. Chem. Int. Ed. 57 (2018) 16339–16342.

[48] F. Pan, H. Zhang, K. Liu, D. Cullen, K. More, M. Wang, Z. Feng, G. Wang, G. Wu, Y. Li, Unveiling active sites of CO_2 reduction on nitrogen-coordinated and atomically dispersed iron and cobalt catalysts, ACS Catal. 8 (2018) 3116–3122.

[49] X. Wang, Z. Chen, X. Zhao, T. Yao, W. Chen, R. You, C. Zhao, G. Wu, J. Wang, W. Huang, Regulation of coordination number over single Co sites: triggering the efficient electroreduction of CO_2, Angew. Chem. 130 (2018) 1962–1966.

[50] D.T. Lee, J.D. Jamir, G.W. Peterson, G.N. Parsons, Protective fabrics: metal-organic framework textiles for rapid photocatalytic sulfur mustard simulant detoxification, Matter 2 (2020) 404–415.

[51] N. Sadeghi, S. Sharifnia, T.-O. Do, Enhanced CO_2 photoreduction by a graphene–porphyrin metal–organic framework under visible light irradiation, J. Mater. Chem. A 6 (2018) 18031–18035.

[52] T. He, S. Chen, B. Ni, Y. Gong, Z. Wu, L. Song, L. Gu, W. Hu, X. Wang, Zirconium–porphyrin-based metal–organic framework hollow nanotubes for immobilization of noble-metal single atoms, Angew. Chem. 130 (2018) 3551–3556.

[53] K.G. Upul Wijayantha, S. Saremi-Yarahmadi, L.M. Peter, Kinetics of oxygen evolution at alpha-Fe_2O_3 photoanodes: a study by photoelectrochemical impedance spectroscopy, Phys. Chem. Chem. Phys. 13 (2011) 5264–5270.

[54] J. Tan, W. Yang, Y. Oh, H. Lee, J. Park, R. Boppella, J. Kim, J. Moon, Fullerene as a photoelectron transfer promoter enabling stable TiO_2-protected Sb_2Se_3 photocathodes for photo-electrochemical water splitting, Adv. Energy Mater. 9 (2019), 1900179.

[55] J. Zhang, R. García-Rodríguez, P. Cameron, S. Eslava, Role of cobalt–iron (oxy) hydroxide ($CoFeO_x$) as oxygen evolution catalyst on hematite photoanodes, Energy Environ. Sci. 11 (2018) 2972–2984.

[56] X. Li, Y. Sun, J. Xu, Y. Shao, J. Wu, X. Xu, Y. Pan, H. Ju, J. Zhu, Y. Xie, Selective visible-light-driven photocatalytic CO_2 reduction to CH_4 mediated by atomically thin $CuIn_5S_8$ Layers, Nat. Energy 4 (2019) 690–699.

[57] T. Wang, X. Meng, P. Li, S. Ouyang, K. Chang, G. Liu, Z. Mei, J. Ye, Photoreduction of CO_2 over the well-crystallized ordered mesoporous TiO_2 with the confined space effect, Nano Energy 9 (2014) 50–60.

[58] N. Ulagappan, H. Frei, Mechanistic study of CO_2 photoreduction in Ti silicalite molecular sieve by FT-IR spectroscopy, J. Phys. Chem. A 104 (2000) 7834–7839.

[59] E.R. Corson, R. Kas, R. Kostecki, J.J. Urban, W.A. Smith, B.D. McCloskey, R. Kortlever, In situ ATR–SEIRAS of carbon dioxide reduction at a plasmonic silver cathode, J. Am. Chem. Soc. 142 (2020) 11750–11762.

[60] M. Huang, B. Deng, X. Zhao, Z. Zhang, F. Li, K. Li, Z. Cui, L. Kong, J. Lu, F. Dong, Template-sacrificing synthesis of well-defined asymmetrically coordinated single-atom catalysts for highly efficient CO_2 electrocatalytic reduction, ACS nano 16 (2022) 2110–2119.

[61] L. Liu, Y. Li, Understanding the reaction mechanism of photocatalytic reduction of CO_2 with H_2O on TiO_2-based photocatalysts: a review, Aerosol Air Qual. Res. 14 (2014) 453–469.
[62] F. Vigier, C. Coutanceau, F. Hahn, E. Belgsir, C. Lamy, On the mechanism of ethanol electro-oxidation on Pt and PtSn catalysts: electrochemical and in situ IR reflectance spectroscopy studies, J. Electroanal. Chem. 563 (2004) 81–89.
[63] Y. Pan, R. Lin, Y. Chen, S. Liu, W. Zhu, X. Cao, W. Chen, K. Wu, W.-C. Cheong, Y. Wang, Design of single-atom Co–N_5 catalytic site: a robust electrocatalyst for CO_2 reduction with nearly 100% CO selectivity and remarkable stability, J. Am. Chem. Soc. 140 (2018) 4218–4221.